The formation of Mg-orthocarbonate through the reaction $MgCO_3 + MgO = Mg_2CO_4$ at Earth's lower mantle P–T conditions

Pavel N. Gavryushkin [*,1,2], Dinara N. Sagatova[1,2], Nursultan Sagatov[1], and Konstantin D. Litasov[3]

[1]*Sobolev Institute of Geology and Mineralogy, Siberian Branch of Russian Academy of Sciences, prosp. acad. Koptyuga 3, 630090 Novosibirsk, Russia*
[2]*Novosibirsk State University, Pirogova 2, Novosibirsk 630090, Russia*
[3]*Vereshchagin Institute for High Pressure Physics RAS, 108840, Troitsk, Moscow, Russian Federation*

Abstract

Orthocarbonates of alkaline earth metals are the newly discovered class of compounds stabilized at high pressures. Mg-orthocarbonates are the potential carbon host phases, transferring oxidized carbon in the Earth's lower mantle up to the core-mantle boundary. Here, we demonstrate the possibility for the formation of Mg_2CO_4 in the lower mantle at pressures above 50 GPa, by *ab initio* calculations. Mg_2CO_4 is formed by the reaction $MgCO_3 + MgO = Mg_2CO_4$, proceeding only at high-temperatures. At 50 GPa the reaction starts at 2200 K. The temperature decreases with pressure and drops down to 1085 K at the pressure of the Earth's core-mantle boundary, near 140 GPa. Two stable structures, Mg_2CO_4-*Pnma* and Mg_2CO_4-*P2$_1$/c*, were revealed. Mg_2CO_4-*Pnma* is isostructural to forsterite (Mg_2SiO_4), while Mg_2CO_4-*P2$_1$/c* is isostructural to larnite (β-Ca_2SiO_4). Transition pressure from Mg_2CO_4-*Pnma* to Mg_2CO_4-*P2$_1$/c* is around 80 GPa. Both phases are dynmaically stable on decompression down to the ambient pressure and can be presreved in the samples of natural high-pressure rocks or the proructs of experiments. Mg_2CO_4-*Pnma* has a melting temperature more than 16% higher than the melting temperature of magnesite ($MgCO_3$). At 23.7 GPa, 35.5 GPa, and 52.2 GPa, Mg_2CO_4-*Pnma* melts at 2661 K, 2819 K, and 3109 K, respectively.

[*]Electronic address: `gavryushkin@igm.nsc.ru`, `p.gavryushkin@g.nsu.ru`; Corresponding author

1

Acoustic wave velocities Vp and Vs of Mg$_2$CO$_4$-*Pnma* are very similar to that of magnesite, while universal anisotropy of Mg$_2$CO$_4$-*Pnma* is stronger than that of magnesite, as well as coefficient A^U is larger for orthocarboante. Calculated Raman spectra of Mg$_2$CO$_4$-*Pnma* will help its identification in high pressure experiments.

Introduction

During the recent decade, the crystal structure prediction technique became an integral part of high-pressure research. Numerous experimental synthesis were guided by this technique, for instance, the synthesis of the high-pressure phases of alkaline [1–3] and alkaline earth carbonates [4–10]. Orthocarbonates of alkaline earth metals are another example for experimental confirmation of theoretically predicted structures.

For the long time, Mg-orthocarbonate atracted attention of the Earth scientists as the possible phase of the deep Earth's interiors. To the best of our knowledge, the formation of Mg$_2$CO$_4$ phase with spinel structure through the reaction MgCO$_3$ + MgO = Mg$_2$CO$_4$ was first suggested by Fyfe in 1970 [11]. Then possibility of this reaction has been hypothesized by Irwing and Wyllie in 1973 [12], and by T. Katsura in 1991 [13]. However, recently performed *ab initio* crystal structure prediction calculations have not found any structures of Mg$_2$CO$_4$ stable at pressures of the Earth's mantle [14]. The enthalpies of all the found structures were lower then the enthlpy of the mechanical mixture of MgCO$_3$+MgO, i.e. they are thrmodynamically unstable.

Our calculations on crystal structure prediction have revealed stable crystal structures of Ca-, Sr-, and -Ba, orthocarboates, Ca$_2$CO$_4$ [15], Sr$_2$CO$_4$ [16], and Ba$_2$CO$_4$ [16]. Subsequent experimental synthesis have confirmed existence of Ca$_2$CO$_4$ and Sr$_2$CO$_4$ [17,18]. Thus, Mg$_2$CO$_4$ remains the sole representative of alkaline earth orthocarboantes for which stable structures are not known.

In the present work, we continue our investgation of orthocarboates, find stable strutures of Mg$_2$CO$_4$, calculate their metling temperatures, seismic properties and P–T phase diagram, as well as Raman spectra for the identification in high-pressure experiments, which are currently underway.

Methods

To increase the chances for finding the energetically favorable structures we have used both USPEX and AIRSS methods, each of which has apparent advantages [19]. *Ab initio* structure prediction was complemented by the prediction technique based on the known structures of Mg- and Zn- orthosilicates with isolated [SiO$_4$] tetrahedrons, as well as sulfates with isolated [SO$_4$] tetrahedrons. Mg$_2$CO$_4$ structures were produced from these structures by the corresponding replacement of the cations and consequent local optimizations. The following crystal structures have been used (numbers in parentheses indicate

the number of formula units (f.u.) in the unit cell): ringwodite (Mg_2SiO_4-$Fd\bar{3}m$ (8)), porierite (Mg_2SiO_4-$Pmma$ (4)), wadsleyite (Mg_2SiO_4-$Imma$ (8)), forsterite (Mg_2SiO_4-$Pnma$ (4)) [20], Zn_2SiO_4-$Pbca$ (8), Zn_2SiO_4-$I\bar{4}2d$ (4) [21], Na_2SO_4-$Fddd$ (8) [22], Li_2SO_4-$P2_1/c$ (4) [23], and Ca_2CO_4-$Pnma$ (4) [15].

The calculations with the USPEX method [24–27] have been performed for 1-4 f.u. of Mg_2CO_4 at 25, 50, and 100 GPa. The seeding technique, implemented in version 10.2 of the USPEX, has been employed in all calculations. The aforementioned structures based on silicates, sulfates, and orthocarbonate have been used as the seeds. Totally, around 3000 structures have been calculated at each pressure. Crystal structure prediction with AIRSS 0.9.1 [28, 29] has been performed only at 50 GPa for 2, 3, and 4 f.u. and a total of nearly 4000 structures have been generated in this calculation.

The energetic optimizations of the predicted structures have been performed within density functional theory (DFT), implemented in the VASP package [30, 31].

To take into account the temperature effect and calculate P–T phase diagram, we used the lattice dynamics method within the quasi-harmonic approximation (QHA). For this task, the lattice vibration frequencies were calculated with the PHONOPY code [32]. By our experience with P–T phase diagrams of carbonates, this technique reliably reproduces phase boundaries in the wide temperature range [2, 15, 33], up to 80-90 % of the melting temperature, if the process of dynamical disordering does not take place.

Melting temperatures of the predicted structures have been determined, using the so-called *Z-method*, based on the molecular dynamic (MD) simulations [34].

To determine the wave velocities V_p and V_s and assess anisotropy of Mg-orthocarbonates, static elastic stiffness tensor (C_{ij}) was calculated from the stress (σ)- strain (ϵ) relation $\sigma_i = C_{ij}\epsilon_j$. Based on these C_{ij} data, we calculated averages of bulk (B) and shear (G) moduli using the Voigt-Ruess-Hill scheme [35, 36]. Then we have determined compression (A_B), shear (A_G), and universal anisotropy (A^U) indexes.

The details of DFT, crystal structure predictions, thermodynamic and elastic property calculations, and MD simulations are given in *Supporting information*.

In order to obtain the Raman spectra the polarizability tensors for each crystal mode were calculated using the *vasp_raman.py* code [37]. The atomic charges were analyzed by the grid-based bader analysis algorithm [38, 39], in which the grid is obtained by decomposition of the charge density by the static self-consistent calculation for the optimized structures. FindSym program [40] and instruments of Phonopy package have been used for the symmetry determination. VESTA and ToposPro [41, 42] programs have been used for the visualization of the crystal structures and figures preparation. The topology of the structures was analysed with ToposPro and Robocrystallographer programs [42, 43].

Results and discussion

Predicted structures

In the crystal structure prediction calculations at 25 and 50 GPa, USPEX has revealed the Mg_2CO_4-$Pnma$ structure as the most energetically favorable. This structure has lower enthalpy than Mg_2CO_4-Cm, predicted by AIRSS, and structures, obtained based on the crystal structures of silicates and sulfates (Figure 1 and S1).

At 100 GPa, USPEX has found another favorable structure with monoclinic symmetry, Mg_2CO_4-$P2_1/c$. The transition from Mg_2CO_4-$Pnma$ to Mg_2CO_4-$P2_1/c$ occurs at 52 GPa, and at higher pressures Mg_2CO_4-$P2_1/c$ is the most energetically favorable among considered structures (Figure 1 and S1).
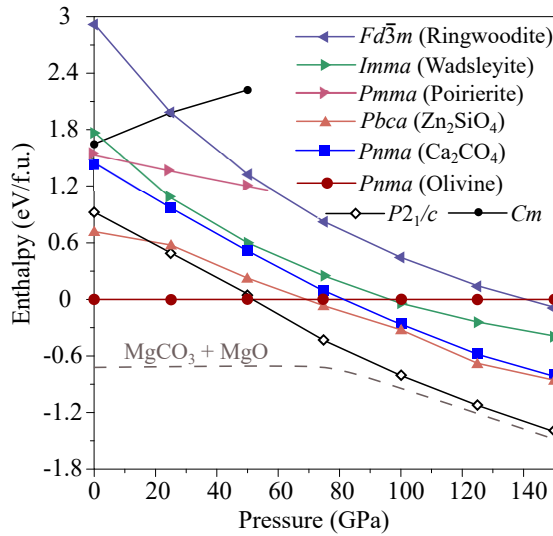

Figure 1: Enthalpy-pressure dependencies of Mg_2CO_4 structures. Isostructural compounds are indicated in brackets.

Revealed Mg_2CO_4-$Pnma$ is isostructural to the mineral forsterite (Figure 2a,b). Atoms in both positions Mg(1) and Mg(2) are 6-coordinated, with the octahedral coordination polyhedron (Figure 2c). Mg_2CO_4-$P2_1/c$ is isostructural to β-Ca_2SiO_4 (larnite) and can be considered as the monoclinic analogue of Ca_2CO_4-$Pnma$. In crystal structure of Mg_2CO_4-$P2_1/c$, there are two non-equivalent Mg sites. There is some ambiguity in determination of cooridnation numbers of Mg, due to the smooth variation of the bonds lengths. In the first site Mg(1) is bonded to six oxygen atoms, arranged in highly deformed trigonal prism (Figure 2d). Lengths of the six Mg–O bonds within coordination polyhedron vary in the range 1.832–2.073 Å, while the seventh oxygen atoms is distant on 2.382 Å. In the second site, Mg(2) is bonded to eight oxygen atoms, forming relatively regular square antiprism. Lengths of these eight Mg–O bonds

vary in the range of 1.887–2.126 Å, while the neinth Mg–O bond is sufficiently longer, being equal to 2.688 Å. For comparison, in Mg_2CO_4-$Pnma$ structure, oxygen atoms in the first coordination sphere is distant on 1,815–1.888 Å for Mg(1) site and on 1.781–1.95 Å — for (Mg2) site. All the presented bond lengths corresond to the pressure of 100 GPa. In both $Pnma$ and $P2_1/c$ crystal structures, coordination polyhedrons around Mg atoms share both vertices and edges with [CO_4] tetrahedrons (Figure 2c,d). Transition from Mg_2CO_4-$Pnma$ to Mg_2CO_4-$P2_1/c$ is accompanied by the sufficient decrease of the volume equal to 5.7 % (Figure S2).

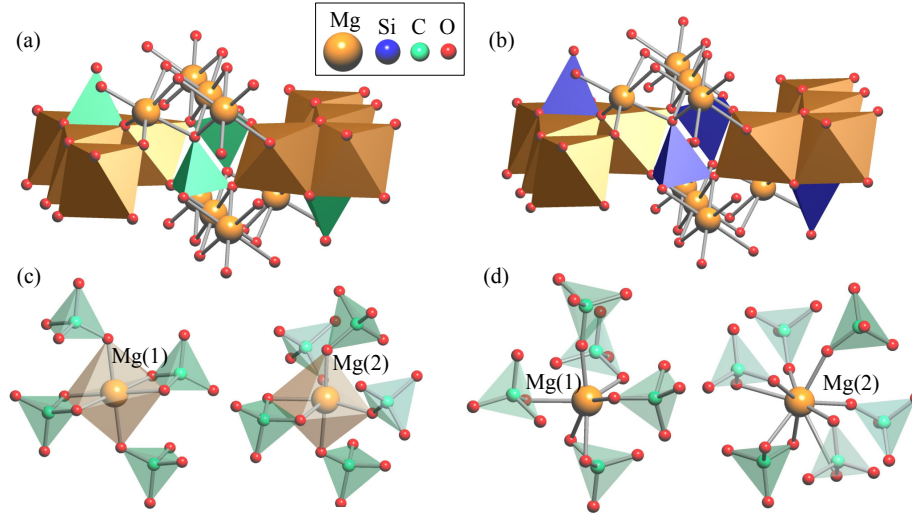Figure 2: Comparison of crystal structures of Mg_2CO_4-$Pnma$ (a) and Mg_2SiO_4-$Pnma$ (b) in projection on the (010) plane, coordination environment around Mg(1) and Mg(2) sites in crystals structures Mg_2CO_4-$Pnma$ (c) and Mg_2CO_4-$P2_1/c$ (d).

Structural data for the Mg_2CO_4-$Pnma$ and Mg_2CO_4-$P2_1/c$ are given in the Table 1. Both structures are dynamically stable in the investigated pressure range 0-140 GPa, and there are no imaginary frequencies in their phonon dispersion curves (Figure 3, S3). The dynamical stability of the found Mg_2CO_4 structures at ambient pressure assume the possibility for their extraction from the chamber of the diamond anvill cell (DAC) after the high pressure synthesis and the further investgation with the technique of transmission electron microscopy. In the *Supporting information*, we have also shown phonon dispersion curves of $MgCO_3$ and MgO (Figure S4) used for the construction of P–T phase diagram.

Table 1: Structural data of predicted Mg_2CO_4 phases at 0 K.

P (GPa)	Space group	Lattice parameters (Å, deg)			Atom	Coordinates		
						x	y	z
50	$Pnma$ (#62)	$a = 8.926$	$b = 5.565$	$c = 4.221$	Mg1	0.000	0.000	0.500
		$\alpha = 90.0$	$\beta = 90.0$	$\gamma = 90.0$	Mg2	0.721	0.250	0.531
					C1	-0.097	0.250	0.087
					O1	-0.091	0.250	0.770
					O2	0.548	0.250	0.284
					O3	0.169	0.552	0.786
100	$P2_1/c$ (#14)	$a = 4.408$	$b = 5.383$	$c = 8.345$	Mg1	0.702	0.360	0.425
		$\alpha = 90.0$	$\beta = 117.65$	$\gamma = 90.0$	Mg2	-0.022	0.000	0.693
					C1	0.355	0.282	0.082
					O1	0.146	0.334	0.638
					O2	0.681	0.245	0.197
					O3	0.272	0.168	-0.080
					O4	0.295	0.520	0.064
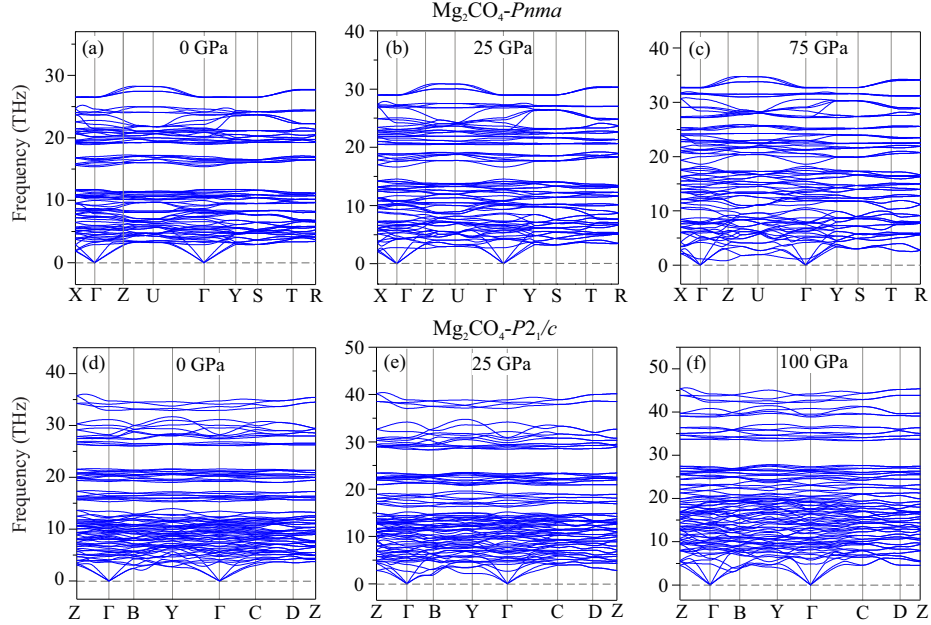
Figure 3: Phonon dispersion curves of Mg_2CO_4-$Pnma$ (a-c) and Mg_2CO_4-$P2_1/c$ (d-f) at various pressures and 0 K.

There is no analogy of the found transition from Mg_2CO_4-$Pnma$ to Mg_2CO_4-$P2_1/c$ in the Mg_2SiO_4 system. However, there is one in Ca_2SiO_4 system, where transformation of Mg_2CO_4-$Pnma$ into Mg_2CO_4-$P2_1/c$ corresponds to

the transforamtion of γ-Ca_2SiO_4 into β-Ca_2SiO_4, which is alsi realized on compression [44]. Heating of β-Ca_2SiO_4 produces the phase α'_H-Ca_2SiO_4 and similar transition can be suggested for Mg_2CO_4. In this case, heating of Mg_2CO_4-$P2_1/c$ will produce the new hypothetical phase Mg_2CO_4-$Pnma$-II similar to α'_H-Ca_2SiO_4. The performed calculations of phonon dispersion curves of Mg_2CO_4-$Pnma$-II, constructed based on the structure of α'_H-Ca_2SiO_4 by corresponding atomic replacements, have shown the dynamical instability of this phase (Figure S6). However, the stabilization of the structure by the factors, which are not considered within QHA can not be excluded.

P–T phase diagram

The performed enthalpy calculations of the Mg_2CO_4, MgO, and $MgCO_3$ structures have shown, that both Mg_2CO_4-$Pnma$ and Mg_2CO_4-$P2_1/c$ lie above the energetic convex hull, i.e. they are unstable and decompose to the mixture (MgO+$MgCO_3$) at 0 K (Figure S7).

However, performed calculations of the Gibbs free energies in the temperature range of 0–3000 K have shown that above some temperature Mg_2CO_4 became more energetically favorable than the (MgO+$MgCO_3$) mixture (Figure S8). At 20 GPa, this temperature is 2420 K, which is nearly equal to the melting temperature of magnesite ($MgCO_3$-$R\bar{3}c$) [45] (Figure 4). With increasing the pressure the temperature of transition decreases, and at 140 GPa Mg_2CO_4-$P2_1/c$ became more favourable than the mixture of (MgO+$MgCO_3$) at temperatures higher than 1085 K. Thus, in the pressure range of 50–140 GPa, Mg_2CO_4 can be synthesised at temperatures 250–1100 K higher than the corresponding temperatures of $MgCO_3$ melting (Figure 4). It suggests the possibility for the formation of Mg-orthocarbonate in most part of the Earth's lower mantle, at pressures higher than 50 GPa.
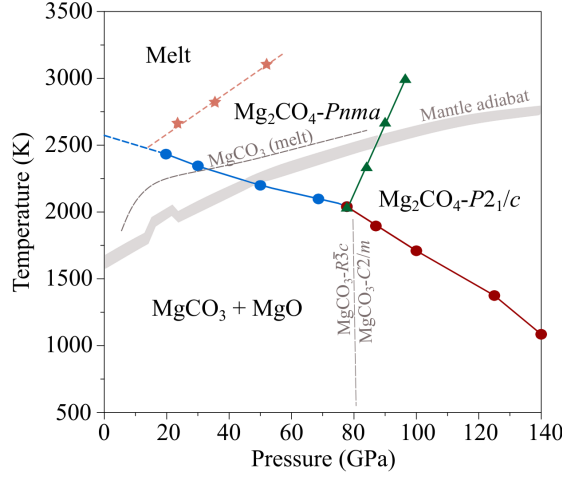
Figure 4: *P–T* phase diagram of Mg_2CO_4. The asterisks represent calculated melting temperatures; the grey dash-dotted line — calculated phase transition boundary of $MgCO_3$; the grey dashed line — melting curve of $MgCO_3$ as reported by Solopova et al. [45]; grey solid line — mantle adiabat according to Katsura [46].

Raman spectra

As Raman techniqe are now actively used for the identification of sp^3 bonded carbonates and orthocarbonates in high-pressure DAC experiments [47, 48], we have calculted Raman spectra for the Mg_2CO_4-*Pnma* phase.

The unit cells of Mg_2CO_4-*Pnma* contain 28 atoms, i.e. there are 84 phonon modes. According to a group theoretical analysis, 36 Raman active modes are expected for Mg_2CO_4-*Pnma*: $\Gamma = 11A_g + 7B_{1g} + 11B_{2g} + 7B_{3g}$. The most intense mode (B_{2g}) corresponds to the bending and stretching vibrations in the [CO_4] tetrahedral groups and appears at 1025 cm^{-1}. The second (A_g) and third (B_{1g}) most intense modes appear at 1089 and 1106 cm^{-1}, correspondingly (Figure 5). The calculated Raman spectra at 60 GPa is shown in Figure 6.
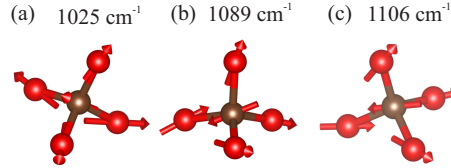

Figure 5: Displacement patterns in Raman modes of Mg_2CO_4-*Pnma* at 60 GPa. Arrows indicate the displacement of the atoms during the specific vibration.
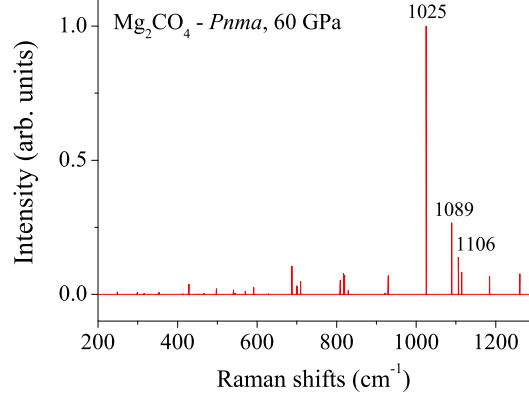
Figure 6: DFT-calculated Raman spectra of Mg_2CO_4-$Pnma$ at 60 GPa.

Analysis of electronic denisty distribution

In both found structures, $Pnma$ and $P2_1/c$, four C–O bonds within $[CO_4]$ tetrahedron are of nearly the same length. At 100 GPa, these bond distances vary in the range 1.32–1.37 Å in both structures. The similar values of bond lengths assume the covalent nature for all four bonds. The performed analysis of electron density distribution confirms this assumption. The isosurface of the electron desity difference clearly shows the accumulation of charge halfway along each of the four C—O bond (Figure 7).
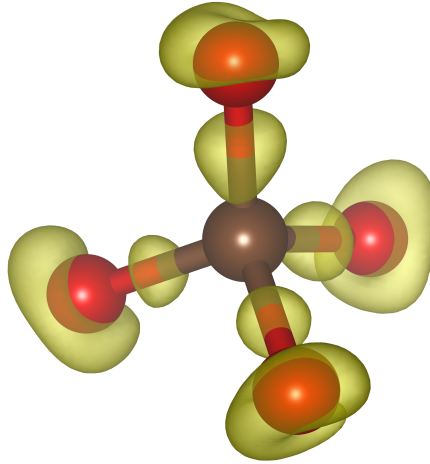

Figure 7: Isosurface of the electron density difference in Mg_2CO_4-$Pnma$ structure. The isosurface shows those regions in which the electron density is larger than that obtained by overlapping electron densities of non-interacting atoms.

The isostructural character of Mg_2CO_4-$Pnma$ and Mg_2SiO_4-$Pnma$ gives a rare possibility for performing the comparison of electron density distribution in the structures of orthocarbonate and orthosilicate.

At 0 GPa, the Si–O bond is longer than C–O bond on 15-19 %. According to the classical rule of isomorphism, suggested by Goldschmidt, the isomorphism in the wide range of compositions require the difference of atomic radii on no more than 15 %. The obtained value is on the border of this limit and from the first glance the possibility of the (Si,C) isomorphism at high temperatures can not be excluded. However, it is not the case, as isomorhism requires similar nature of the bonds around atoms substituting each other. The obtained Bader charge of C^{4+} is predictably lower than that of Si^{4+}, 1.914 against 3.109. This indicates on the more covalent character of C–O bond in comparison with the Si–O bond. Bader charges of the other atoms are summarised in Table 2.

Table 2: Comparison of Bader charges on atoms in Mg_2SiO_4-$Pnma$ and Mg_2CO_4-$Pnma$ structures at 0 GPa (in unit of e).

	Mg1	Mg2	C/Si	O1	O2	O3
Mg_2SiO_4	1.731	1.745	3.109	-1.645	-1.657	-1.641
Mg_2CO_4	1.724	1.745	1.914	-1.412	-1.340	-1.315

Melting temperature and seismic properties

To compare the melting temerature of Mg-carboante and Mg-orhtocarboantes, we have estimated melting temperatures of Mg-orthocarbonate. The obtained values of the Mg_2CO_4-$Pnma$ melting temperatures at 23.7 GPa, 35.5 GPa and 52.2 GPa equal to 2661 K, 2819 K, and 3109 K, respectively (Figure S9). These values are 14-22 % higher than the experimentally measured melting temperatures of magnesite and comparable with solidi of silicate rocks under lower mantle P–T conditions [49]. As can be seen from Figure 4 the difference in melting temperatures promptly increases with pressure, reaching 500 K at nearly 40 GPa.

To assess the effect of orthocarbonate formation on the seismic properties of carbonate, we have also calculated the elastic stiffness tensor and compressional/shear sound velocities (V_p/V_s) for Mg-carbonate and Mg-orthocarbonate. We have not aimed the investigation of trends for the changes of elastic properties on compression or their description during $Pnma \rightarrow P2_1/c$ transition, but only the rough comparison of carbonate and orthocarbonate properties. By this reason, calculations have been performed only at 50 GPa and 0 K for Mg_2CO_4-$Pnma$ and magnesite structures.

The obtained elastic properties of Mg_2CO_4-$Pnma$ and magnesite are summarized in Table S1 and Table S2. Obtained values of C_{ij}, B, G, V_p, and V_s for magnesite are in good agreement with the previous results of theoretical calculations [50]. According to our results, the density and both bulk and shear moduli of Mg_2CO_4-$Pnma$ are higher than that of magnesite by 4-5 %. Orthocarbonate

is similar to carbonate in sense of seismic velocities V_p and V_s, but orthocarbonate is more anisotropic, owning higher universal anisotropy (A^U). The value of A^U for Mg_2CO_4-$Pnma$ is 0.4772, while that for magnesite is 0.2838.

Acknowledgments

References

[1] Gavryushkin, P. N.; Behtenova, A.; Popov, Z. I.; Bakakin, V. V.; Likhacheva, A. Y.; Litasov, K. D.; Gavryushkin, A. Toward analysis of structural changes common for alkaline carbonates and binary compounds: prediction of high-pressure structures of Li_2CO_3, Na_2CO_3, and K_2CO_3. *Crystal Growth & Design 16*, **2016**, 5612–5617.

[2] Gavryushkin, P. N.; Bekhtenova, A.; Lobanov, S. S.; Shatskiy, A.; Likhacheva, A. Y.; Sagatova, D.; Sagatov, N.; Rashchenko, S. V.; Litasov, K. D.; Sharygin, I. S.; et al. High-pressure phase diagrams of Na_2CO_3 and K_2CO_3. *Minerals 9*, **2019**, 599.

[3] Grzechnik, A.; Bouvier, P.; Farina, L. High-pressure structure of Li_2CO_3. *Journal of Solid State Chemistry 173*, **2003**, 13–19.

[4] Oganov, A. R.; Glass, C. W.; Ono, S. High-pressure phases of $CaCO_3$: Crystal structure prediction and experiment. *Earth and Planetary Science Letters 241*, **2006**, 95 – 103.

[5] Pickard, C. J.; Needs, R. J. Structures and stability of calcium and magnesium carbonates at mantle pressures. *Physical Review B 91*, **2015**, 104101.

[6] Gavryushkin, P. N.; Martirosyan, N. S.; Inerbaev, T. M.; Popov, Z. I.; Rashchenko, S. V.; Likhacheva, A. Y.; Lobanov, S. S.; Goncharov, A. F.; Prakapenka, V. B.; Litasov, K. D. Aragonite-II and $CaCO_3$-VII: New high-pressure, high-temperature polymorphs of $CaCO_3$. *Crystal Growth & Design 17*, **2017**, 6291–6296.

[7] Smith, D.; Lawler, K. V.; Martinez-Canales, M.; Daykin, A. W.; Fussell, Z.; Smith, G. A.; Childs, C.; Smith, J. S.; Pickard, C. J.; Salamat, A. Postaragonite phases of $CaCO_3$ at lower mantle pressures. *Physical Review Materials 2*, **2018**, 013605.

[8] Solomatova, N. V.; Asimow, P. D. First-principles calculations of high-pressure iron-bearing monoclinic dolomite and single-cation carbonates with internally consistent hubbard u. *Physics and Chemistry of Minerals* **2017**, 1–10.

[9] Binck, J.; Chariton, S.; Stekiel, M.; Bayarjargal, L.; Morgenroth, W.; Milman, V.; Dubrovinsky, L.; Winkler, B. High-pressure, high-temperature phase stability of iron-poor dolomite and the structures of dolomite-IIIc and dolomite-V. *Physics of the Earth and Planetary Interiors 299*, **2020**, 106403.

[10] Merlini, M.; Cerantola, V.; Gatta, G. D.; Gemmi, M.; Hanfland, M.; Kupenko, I.; Lotti, P.; Müller, H.; Zhang, L. Dolomite-IV: Candidate structure for a carbonate in the earth's lower mantle. *American Mineralogist 102*, **2017**, 1763–1766.

[11] Fyfe, W. Lattice energies, phase transformations and volatiles in the mantle. *Physics of the Earth and Planetary Interiors 3*, **1970**, 196–200.

[12] Irving, A.; Wyllie, P. Melting relationships in CaO-CO_2 and Mgo-CO_2 to 36 kilobars with comments on CO_2 in the mantle. *Earth and Planetary Science Letters 20*, **1973**, 220–225.

[13] Katsura, T.; Tsuchida, Y.; Ito, E.; Yagi, T.; Utsumi, W.; Akimoto, S.-i. Stability of magnesite under the lower mantle conditions. *Proceedings of the Japan Academy, Series B 67*, **1991**, 57–60.

[14] Yao, X.; Xie, C.; Dong, X.; Oganov, A. R.; Zeng, Q. Novel high-pressure calcium carbonates. *Physical Review B 98*, **2018**, 014108.

[15] Sagatova, D.; Shatskiy, A.; Sagatov, N.; Gavryushkin, P. N.; Litasov, K. D. Calcium orthocarbonate, Ca_2CO_4-*Pnma*: A potential host for subducting carbon in the transition zone and lower mantle. *Lithos 370-371*, **2020**, 105637.

[16] Gavryushkin, P. N.; Sagatova, D.; Sagatov, N.; Banaev, M. V. Silicate-like crystallchemistry for carbonates at high pressure. Reality or not? *IV Conference and School for Young Scientists Non-Ambient Diffraction and Nanomaterials (Book of abstracts, 19-21.10.2020)* **2020**, 38.

[17] Laniel, D.; Binck, J.; Winkler, B.; Vogel, S.; Fedotenko, T.; Chariton, S.; Prakapenka, V.; Milman, V.; Schnick, W.; Dubrovinsky, L.; Dubrovinskaia, N. Synthesis, crystal structure and structure–property relations of strontium orthocarbonate, Sr_2CO_4. *Acta Crystallographica Section B 77*, **2021**, 131–137.

[18] Binck, J.; Laniel, D.; L., B.; Khandarkhaeva, S.; Fedotenko, T.; Aslandukov, A.; Glazyrin, K.; Milman, V.; Chariton, S.; Prakapenka, V. B.;

Dubrovinskaia, N.; Dubrovinsky, L.; Winkler, B. Synthesis of calcium orthocarbonate, Ca_2CO_4-Pnma, at p,t-conditions of earth's tramsition zone and lower mantle. *Am. Mineral.* .

[19] Oganov, A. R.; Pickard, C. J.; Zhu, Q.; Needs, R. J. Structure prediction drives materials discovery. *Nature Reviews Materials 4*, **2019**, 331–348.

[20] Smyth, J. R.; Hazen, R. M. The crystal structures of forsterite and hortonolite at several temperatures up to 900 C. *American Mineralogist 58*, **1973**, 588–593.

[21] Kanzaki, M. High-pressure phase relations in Zn_2SiO_4 system: A first-principles study. *arXiv preprint arXiv:1903.05339* **2019**.

[22] Hawthorne, F. C.; Ferguson, R. B. Anhydrous sulphates; I, Refinement of the crystal structure of celestite with an appendix on the structure of thenardite. *The Canadian Mineralogist 13*, **1975**, 181–187.

[23] Alcock, N. W.; Evans, D. A.; Jenkins, H. D. B. Lithium sulphate – a redetermination. *Acta Crystallographica Section B 29*, **1973**, 360–361.

[24] Oganov, A. R.; Glass, C. W. Crystal structure prediction using ab initio evolutionary techniques: Principles and applications. *The Journal of Chemical Physics 124*, **2006**, 244704.

[25] Oganov, A. R.; Lyakhov, A. O.; Valle, M. How evolutionary crystal structure prediction works—and why. *Accounts of Chemical Research 44*, **2011**, 227–237. PMID: 21361336.

[26] Lyakhov, A. O.; Oganov, A. R.; Stokes, H. T.; Zhu, Q. New developments in evolutionary structure prediction algorithm uspex. *Computer Physics Communications 184*, **2013**, 1172 – 1182.

[27] Bushlanov, P. V.; Blatov, V. A.; Oganov, A. R. Topology-based crystal structure generator. *Computer Physics Communications 236*, **2019**, 1 – 7.

[28] Pickard, C. J.; Needs, R. J. High-pressure phases of silane. *Physical Review Letters 97*, **2006**, 045504.

[29] Pickard, C. J.; Needs, R. J. Ab initio random structure searching. *Journal of Physics: Condensed Matter 23*, **2011**, 053201.

[30] Kresse, G.; Furthmüller, J. Efficient iterative schemes for ab initio total-energy calculations using a plane-wave basis set. *Phyical Review B 54*, **1996**, 11169–11186.

[31] Kresse, G.; Furthmüller, J. Efficiency of ab-initio total energy calculations for metals and semiconductors using a plane-wave basis set. *Computational Materials Science 6*, **1996**, 15 – 50.

[32] Togo, A.; Tanaka, I. First principles phonon calculations in materials science. *Scripta Materialia 108*, **2015**, 1–5.

[33] Gavryushkin, P. N.; Sagatov, N.; Belonoshko, A. B.; Banaev, M. V.; Litasov, K. D. Disordered aragonite: The new high-pressure, high-temperature phase of $CaCO_3$. *The Journal of Physical Chemistry C 124*, **2020**, 26467–26473.

[34] Belonoshko, A. B.; Skorodumova, N. V.; Rosengren, A.; Johansson, B. Melting and critical superheating. *Physical Review B 73*, **2006**, 012201.

[35] Hill, R. The elastic behaviour of a crystalline aggregate. *Proceedings of the Physical Society. Section A 65*, **1952**, 349–354.

[36] Hill, R. Elastic properties of reinforced solids: Some theoretical principles. *Journal of the Mechanics and Physics of Solids 11*, **1963**, 357 – 372.

[37] Fonari, A.; Stauffer, S. *vasp_raman.py*. https://github.com/raman-sc/VASP/, **2013**.

[38] Tang, W.; Sanville, E.; Henkelman, G. A grid-based bader analysis algorithm without lattice bias. *Journal of Physics: Condensed Matter 21*, **2009**, 084204.

[39] Henkelman, G.; Arnaldsson, A.; Jónsson, H. A fast and robust algorithm for bader decomposition of charge density. *Computational Materials Science 36*, **2006**, 354–360.

[40] Stokes, H. T.; Hatch, D. M. FINDSYM: program for identifying the space-group symmetry of a crystal. *Journal of Applied Crystallography 38*, **2005**, 237–238.

[41] Momma, K.; Izumi, F. VESTA 3 for three-dimensional visualization of crystal, volumetric and morphology data. *J. Appl. Crystallogr. 44*, **2011**, 1272–1276.

[42] Blatov, V. A.; Shevchenko, A. P.; Proserpio, D. M. Applied topological analysis of crystal structures with the program package ToposPro. *Crystal Growth & Design 14*, **2014**, 3576–3586.

[43] Ganose, A. M.; Jain, A. Robocrystallographer: automated crystal structure text descriptions and analysis. *MRS Communications 9*, **2019**, 874–881.

[44] Belmonte, D.; Ottonello, G.; Zuccolini, M. V. Ab initio-assisted assessment of the $CaO-SiO_2$ system under pressure. *Calphad 59*, **2017**, 12 – 30.

[45] Solopova, N. A.; Dubrovinsky, L.; Spivak, A. V.; Litvin, Y. A.; Dubrovinskaia, N. Melting and decomposition of $MgCO_3$ at pressures up to 84 GPa. *Physics and Chemistry of Minerals 42*, **2015**, 73–81.

[46] Katsura, T.; Yoneda, A.; Yamazaki, D.; Yoshino, T.; Ito, E. Adiabatic temperature profile in the mantle. *Physics of the Earth and Planetary Interiors 183*, **2010**, 212 – 218. Special Issue on Deep Slab and Mantle Dynamics.

[47] Lobanov, S. S.; Dong, X.; Martirosyan, N. S.; Samtsevich, A. I.; Stevanovic, V.; Gavryushkin, P. N.; Litasov, K. D.; Greenberg, E.; Prakapenka, V. B.; Oganov, A. R.; et al. Raman spectroscopy and X-ray diffraction of sp^3 $CaCO_3$ at lower mantle pressures. *Physical Review B 96*, **2017**, 104101.

[48] Binck, J.; Bayarjargal, L.; Lobanov, S. S.; Morgenroth, W.; Luchitskaia, R.; Pickard, C. J.; Milman, V.; Refson, K.; Jochym, D. B.; Byrne, P.; et al. Phase stabilities of $MgCO_3$ and $MgCO_3$-II studied by Raman spectroscopy, X-ray diffraction, and density functional theory calculations. *Physical Review Materials 4*, **2020**, 055001.

[49] Litasov, K. D.; Shatskiy, A. Carbon-bearing magmas in the earth's deep interior. In *Magmas Under Pressure*. Elsevier, **2018**, pages 43–82.

[50] Li, Z.; Stackhouse, S. Iron-rich carbonates stabilized by magnetic entropy at lower mantle conditions. *Earth and Planetary Science Letters 531*, **2020**, 115959.